

# Novel High Frequency Electric Field Sweeping Concept for High Power Gyrotron Collectors

Benjamin Ell, Chuanren Wu, Gerd Gantenbein, Stefan Illy, Moritz Misko, Ioannis Gr. Pagonakis, Manfred Thumm, *Life Fellow, IEEE*, and John Jelonnek, *Senior Member, IEEE*

**Abstract**—Future fusion power plants will require for plasma heating and non-inductive current drive high-power gyrotrons, each of which generates 2 MW of continuous-wave microwave power, while another 2 MW in the spent electron beam is dissipated as heat on the collector wall. In today's 1 MW continuous-wave gyrotrons, collector coils superimpose an AC (10–50 Hz) magnetic field to sweep the hot spots of spent electrons over a large area. However, to double today's power, it will be critical also to reduce the hot spot dwell time preventing significant increase of material fatigue. This can be achieved by increasing the sweeping frequency. However, a higher-frequency magnetic field would hardly penetrate the metallic collector vessel due to eddy currents. Instead of magnetic field, sweeping with electric fields is proposed for the first time. The presented mechanism is capable to apply a several orders higher sweeping frequency to reduce the periodic variation of temperature, thus, the device lifetime can be extended.

**Index Terms**—Electron beams, Gyrotrons

## I. INTRODUCTION

Gyrotrons are vacuum electron tube oscillators with operation frequencies of a few hundred GHz and up to 2 MW of microwave output power. High power gyrotrons are essential for electron cyclotron heating (ECH) and non-inductive current drive (CD) in plasmas of nuclear fusion machines where the high microwave power is required in continuous wave (CW) operation. Current gyrotrons with single-stage depressed collectors (SDC) are capable of a total tube efficiency of approximately 50 %. Most of the total losses in the gyrotron occur in the collector at the point where the spent electron beam intersects the collector surface. This area is located at the inner collector wall and is limited to a small size. Therefore, a high instantaneous power loading density is generated by the large power losses combined with the small surface area, which is decreased with increasing collector

radius. However, current high power gyrotron collectors for CW operation are limited to an inner collector radius in the range of 200 – 300 mm for a compromise in size, weight, power loading density and sensitivity to stray magnetic fields. In addition, these collectors are equipped with magnetic field sweeping systems to distribute the high instantaneous thermal loading onto a larger surface for a reduced time averaged thermal loading.

Two different magnetic field sweeping techniques are used in high power gyrotrons, the longitudinal magnetic field sweeping (LMFS) where the electron beam is moved in axial direction [1–2] and the transversal magnetic field sweeping (TMFS) where the electron beam is tilted on the inner collector wall and rotated in azimuthal direction [3–5]. Both sweeping systems are equipped with water cooled normal conducting coils with a few kW of resistive losses in total. The LMFS coils are placed around the copper collector with a sweeping frequency that is limited to around 10 Hz due to high eddy currents, which are induced in the highly conductive copper collector. The TMFS system is usually operated at a higher frequency of 50 Hz since the coils are located around a stainless-steel section below the copper collector to reduce the shielding effect of eddy currents. Nevertheless, eddy currents are still induced in the less conductive stainless-steel section and the sweeping frequency is limited.

Such low sweeping frequencies are not sufficient for a homogeneous temperature distribution at the inner collector wall due to the high instantaneous thermal power loading. Each point in the intersection region of the inner collector wall with the spent electron beam is rapidly heated when the electron beam is swept over and quickly cooled when the electron beam is at a different position. A higher sweeping frequency could significantly reduce the temperature variation at the inner collector wall and eliminate cyclic fatigue. The reduced peaks of temperature variations on the inner collector wall are no longer the limiting factor for the size of the collector but rather the critical heat flux of the cooling system. Cyclic thermal fatigue is the main limitation in the lifetime of high power gyrotron collectors and will cause cracks and plastic deformation over time.

A sweeping system inside the gyrotron vacuum in close proximity to the electron beam is not limited in the sweeping frequency by eddy currents. However, the operation of a normal conducting coil with significant power consumption is not feasible inside the vacuum tube due to the thermal management of the coil. The power consumption of a sweeping

Manuscript received [month] [day], [year]; revised [month] [day], [year]; accepted [month] [day], [year]. Date of publication [month] [day], [year]; date of current version [month] [day], [year]. The review of this paper was arranged by Editor [Name]. (Corresponding author: Benjamin Ell.)

The authors are with the Institute for Pulsed Power and Microwave Technology, Karlsruhe Institute of Technology, 76131 Karlsruhe, Germany (e-mail: Benjamin.Ell@kit.edu; John.Jelonnek@kit.edu).

Color versions of one or more of the figures in this paper are available online at <http://ieeexplore.ieee.org>.

Digital Object Identifier xxxxxxxxxxxxxxxx

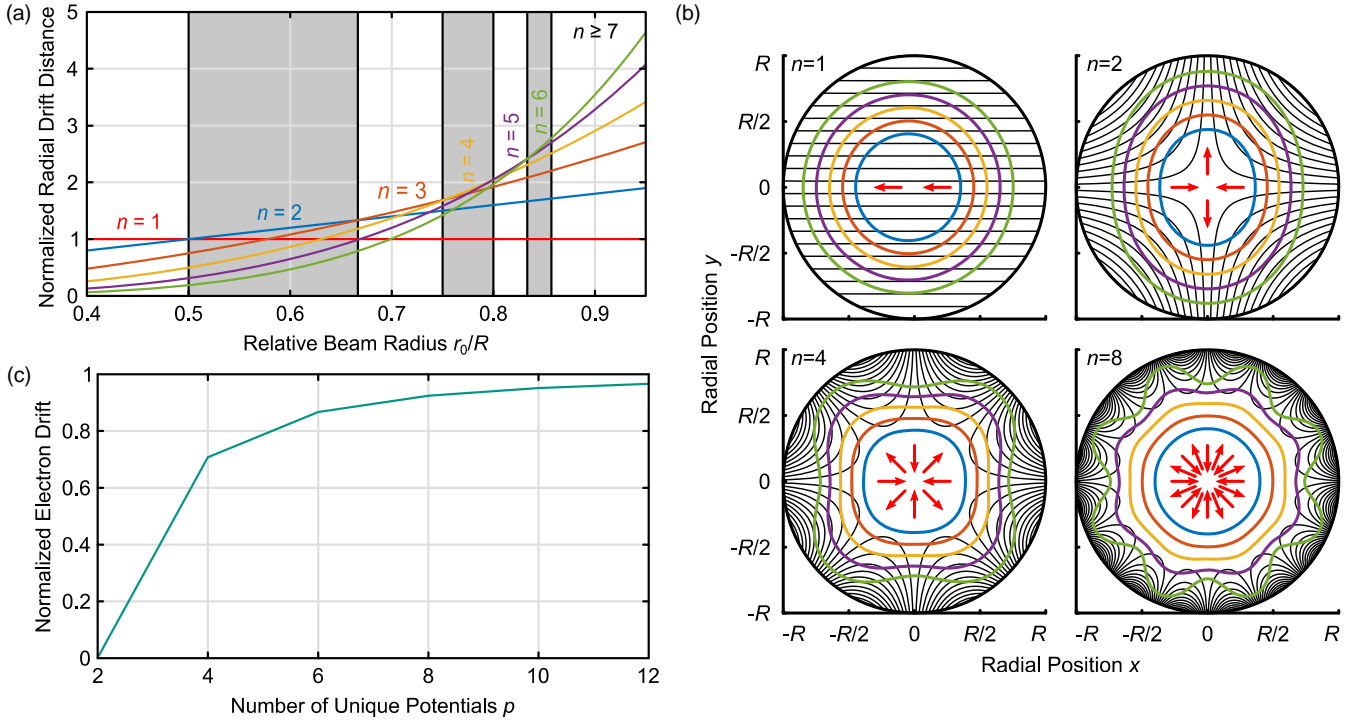


Fig. 1: Parameters for theoretical optimization. (a), Normalized radial electron drift distance in the sweeping region over the relative beam radius for periodic factors of  $n = 1$  to 6. (b), Cross-sections of the electric equipotential lines (black) for periodic factors of  $n = 1, 2, 4, 8$ . Different electron beams are shown after the influence of the sweeping region using  $\tau \gg 0$  with relative beam radii of  $r_0/R = 0.4, 0.5, 0.6, 0.7$  and  $0.8$ . The radial drift direction is represented with arrows in the center of each plot (red). (c), Normalized minimal electron drift distance over the number of unique potentials  $p$ .

system based on an electric field is reduced in comparison to a magnetic field sweeping system.

The spent electron beam in a high power, high frequency gyrotron is confined by a strong magnetic field. A strong electric field perpendicular to the magnetic field is required for modification of the electron trajectories as proposed with the  $E \times B$  drift concept [6]. Static magnetic and electric fields were used in the initial idea to separate the spent beam electrons according to their kinetic energy for an improvement in the collector efficiency. In the present publication, a periodic variation of the electric field and a constant magnetic field is applied for the sweeping of the electron beam in radial direction. The variation in radial direction directly correlates with an axial variation of the intersection region of the electron beam with the cylindrical collector wall. This novel idea of an electric field sweeping system is designed for an SDC where a high collector efficiency is no priority. The main goal of a collector with an electric field sweeping system is the elimination of cyclic fatigue due to higher sweeping frequency and the possibility for smaller collector sizes.

## II. IDEAL MODEL

For simplicity, an ideal two-dimensional model is analyzed in this section to demonstrate the principle. There is a constant axial magnetic field out of the plane of the polar coordinate system. A circular boundary is placed at a radius  $r = R$  with infinite number of electrodes. The electric potential  $\varphi$  on each electrode is a function of the azimuthal angle  $\theta$  and time  $t$ :

$$[\varphi(\theta, t)]_{r=R} = \varphi_0 \cdot \sin\left(n \cdot \theta + 2\pi \cdot \frac{t}{T}\right) \quad (1)$$

where the electric potential  $\varphi_0$  is the amplitude of this periodic setup,  $T$  is the sweeping period and  $n$  is an arbitrary integer for the number of periods. The electric potential in the complete cross-section is solved by the Laplace equation to

$$\varphi(r, \theta, t) = \varphi_0 \cdot \left(\frac{r}{R}\right)^n \cdot \sin\left(n \cdot \theta + 2\pi \cdot \frac{t}{T}\right). \quad (2)$$

The relationship between the electric field  $E$  and the electric potential  $\varphi$  is

$$\vec{E} = -\vec{\nabla}\varphi = -\frac{\partial\varphi}{\partial r} \cdot \vec{r} - \frac{1}{r} \cdot \frac{\partial\varphi}{\partial\theta} \cdot \vec{\theta}. \quad (3)$$

The drift velocity  $\vec{v}_d = \vec{E} \times \vec{B} / |\vec{B}|^2$  of a non-relativistic electron in the axial magnetic field  $\vec{B} = B_0 \cdot \vec{z}$  and the perpendicular electric field from eq. (3) is calculated to

$$\vec{v}_d(r, \theta, t) = -\frac{\varphi_0}{B_0 \cdot R} \cdot n \cdot \left(\frac{r}{R}\right)^{n-1} \cdot \left(\sin\left(n \cdot \theta + 2\pi \cdot \frac{t}{T}\right) \cdot \vec{r} + \cos\left(n \cdot \theta + 2\pi \cdot \frac{t}{T}\right) \cdot \vec{\theta}\right). \quad (4)$$

The maximum radial drift distance  $\Delta r$  of an electron within a short time interval  $\tau \rightarrow 0$  is proportional to

$$\Delta r \propto \tau \cdot n \cdot \left(\frac{r_0}{R}\right)^{n-1}. \quad (5)$$

Equation (5) shows that the effect of the drift becomes more significant with a larger  $\tau$  and also when an electron beam is radially closer to the electrodes. Eq. (5) is visualized in Fig. 1(a) where the number  $n$  is represented by different curves. The radial drift distance is significantly increased for larger  $n$  in combination with an electron beam close to the electrodes. However, the relative beam radius is limited in a realistic design to a value not larger as approximately 0.9 due to tolerances in the magnetic field and misalignments. In this

frame, the maximum reasonable number of repeated potentials in the azimuthal direction is set to  $n = 9$ , as a larger number will not increase the drift distance. Another limitation to  $n$  is the maximum electric field  $E_{\max}$ , which is limited to around 70 – 80 kV/cm to avoid breakdown. The peak to peak potential is limited to the depression potential  $\varphi_{\text{dep}}$  due to axial electric field components of the sweeping structure.

The positions of the beam electrons after the influence of the electric field can be integrated in small time steps. The cross-sections of the electric potential lines (black lines) and electron beams with  $r_0/R = 0.4, 0.5, 0.6, 0.7$  and  $0.8$  are shown in Fig. 1(b) for  $n = 1, 2, 4$  and  $8$ , while the azimuthal positions of a maximum radial drift to the in- and outside are indicated with red arrows. The constant radial position of the electrodes  $R$  is critical for larger initial radii of the electron beams with increasing factor  $n$  due to the reduced distance between the electrodes and the electron beam. This point is addressed in the realistic conceptual design presented in a later section of this manuscript. The electric fields are not varied over time in these calculations due to the condition of a large period length  $T \gg \tau$ . Over a larger time frame with periodic variation of the electric field, the electric fields and the shape of the swept electron beam are rotated along the center point in case of an infinite number of electrodes.

### III. REALISTIC MODEL WITH FINITE NUMBER OF ELECTRODES

A design for an electrical sweeping system with an unlimited number of electrodes is not feasible for a realistic design approach. The number of electrodes  $m$  is defined as  $m = p \cdot n$  where  $n$  is the number of periods and  $p$  is the finite number of unique potentials, in contrast to the ideal model from the previous section corresponding to  $p = \infty$  in which the influence of  $n$  was shown. The maximum electron drift in the cross-section of the electric sweeping system is constant over time for  $p = \infty$  as the maximum potential difference is always  $2 \cdot \varphi_0$ . The influence of a realistic finite value for  $p$  is discussed in this section for even numbers to achieve an average electric potential in the cross-section equal to zero. The electric potentials of the electrodes are defined with eq. (1) at the azimuthal center position of each electrode  $i$  ( $1, \dots, m$ ) which is at an angle of

$$\theta(i) = \frac{2\pi}{n} \cdot \left( \frac{i}{p} - \frac{1}{4} \right). \quad (6)$$

The electric field between the electrodes is dependent on the size and shape of the electrodes however, the absolute electric potential in the center between two neighboring electrodes  $i$  and  $j$  at the radius  $R$  is less than or equal to the absolute average value of both potentials or

$$|\varphi(i, j, t)| \leq \left| \frac{\varphi(\theta(i), t) + \varphi(\theta(j), t)}{2} \right| \quad (7a)$$

$$= \frac{\varphi_0}{2} \cdot \left| \left( \sin \left( n \cdot \theta(i) + 2\pi \cdot \frac{t}{T} \right) + \sin \left( n \cdot \theta(j) + 2\pi \cdot \frac{t}{T} \right) \right) \right| \quad (7b)$$

$$= \varphi_0 \cdot \cos \left( \frac{\pi}{p} \right) \cdot \left| \sin \left( \pi \cdot \left( \frac{i+j}{p} - \frac{1}{2} \right) + 2\pi \cdot \frac{t}{T} \right) \right|. \quad (7c)$$

The maximum possible absolute electric potential  $\varphi_{\max}$  over the period  $T$  at the center position between two neighboring electrodes results to

$$|\varphi_{\max}| \leq \varphi_0 \cdot \cos \left( \frac{\pi}{p} \right). \quad (8)$$

The maximum electron drift in the cross-section of the electric sweeping system over the period  $T$  is minimized when the electric potential at the center position between two neighboring electrodes is maximized.

The normalized maximum possible electron drift at the azimuthal position between two electrodes over the number of unique potentials is shown in Fig. 1(c). It is increased with  $p$  and converges to 1 for  $p = \infty$ , as expected with Eq. (8). The minimal value of  $p$  to achieve an electron drift in the complete cross-section of the sweeping system is four. The difference between the maximum and minimum drift distance in a sweeping cycle is reduced to less than 10 % for  $p \geq 8$ . The complexity of a realistic design approach for an electric field sweeping system is significantly increased with more unique potentials due to the increased number of vacuum feedthroughs for every potential. The number of required power supplies is also increased with  $p$ .

### IV. DEMONSTRATION OF CONCEPT BY A CONCEPTUAL DESIGN

The conceptual design approach of the electric field sweeping system is optimized for the KIT 2 MW 170 GHz coaxial-cavity gyrotron [7]. The nominal depression potential of  $\varphi_{\text{dep}} = -35$  kV as applied in a traditional SDC is used in simulations for the collector with an electric field sweeping system. A 3-D geometry of a collector with an electric field sweeping system is shown in Fig. 2(a). The electrodes for the electric field are axially placed at the entrance of the collector due to the reduced magnetic field for an increased electron drift. The radial center position of the electrodes is set to achieve a relative outside beam radius of 0.85. The maximum possible amplitude of the sweeping potential of  $\varphi_0 = \varphi_{\text{dep}}/2 = 17.5$  kV is applied without exceeding the limit of the breakdown electric field due to the increased radial dimensions at the collector entrance. The magnetic field of the gyrotron magnet is diverged with increasing distance to the cavity along the axis and the radial dimension of the electrodes in axial direction is adapted to the diverging electron beam along the sweeping region. Additional DC collector coils are used to modify the magnetic field in the collector above the electric field sweeping area to reduce the incident angle of the magnetic field lines with the collector wall. The effectiveness of the electric field sweeping system and the electron beam width at the collector wall are increased with a shallower incidence angle. Currents of approximately 5000 Ampere-turns and 2000 Ampere-turns were applied to the lower and upper coil, respectively. The inner radius of the cylindrical copper collector surface was set to 200 mm with a length of 700 mm. The number of repeated potentials is set to  $n = 5$  to achieve an optimal average radial drift distance for the beam electrons with the largest and smallest initial radial position. The number of unique potentials is set to  $p = 8$  for a compromise in a high minimal drift distance and an acceptable complexity with a phase difference of  $45^\circ$ . In total, 40 electrodes are used for the electric field sweeping system. Each electrode is built out of a metallic rod with circular cross-section with a radial dimension of 2 mm. The commercially available voltage feedthroughs are located in  $45^\circ$  angles at the

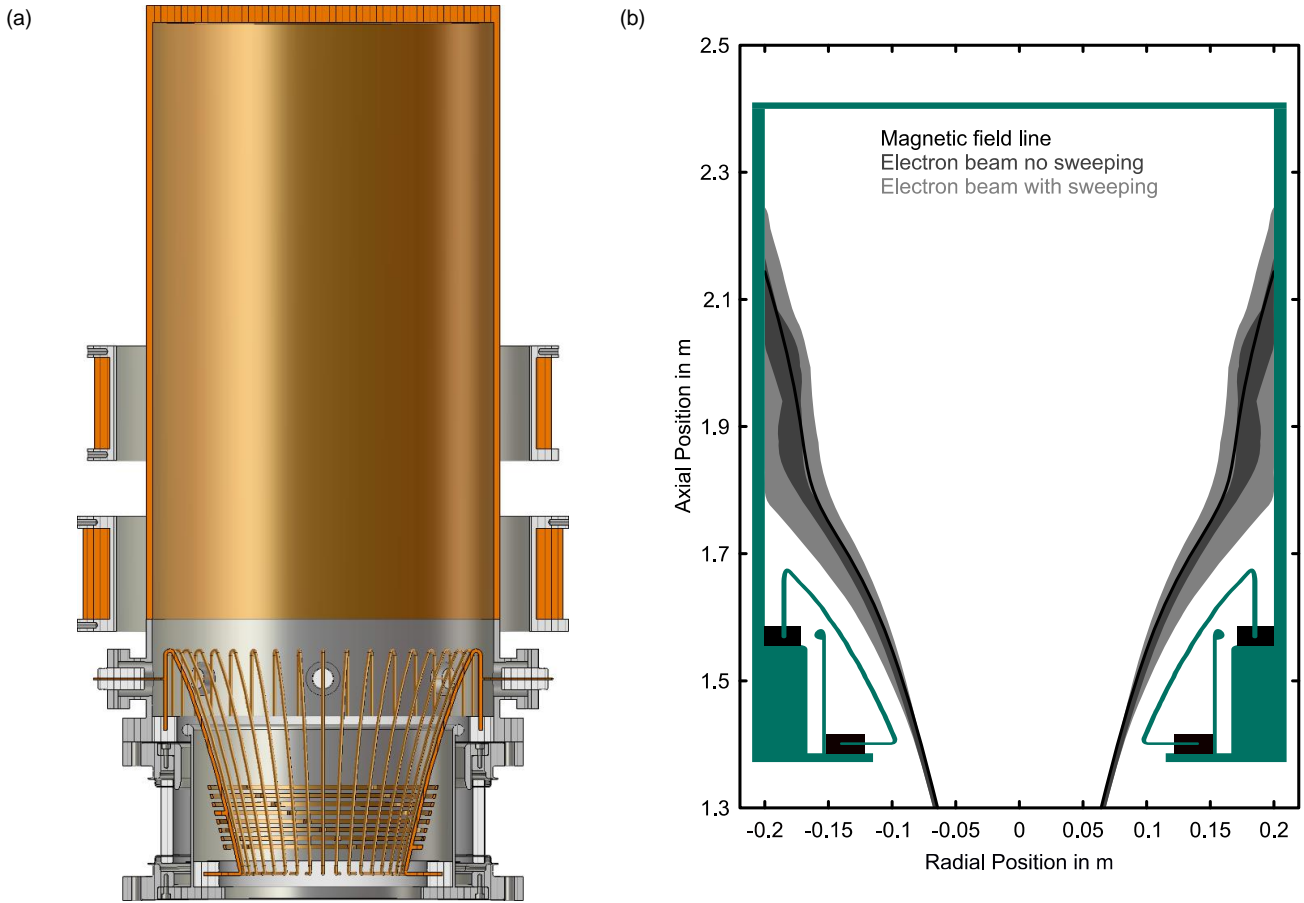


Fig. 2: Conceptual collector design with  $E \times B$  sweeping system. (a), 3D-geometry of a collector with an  $E \times B$  sweeping structure. The periodic factor is set to  $n = 5$  and the number unique potentials to  $p = 8$  for a total of 40 electrodes. (b), Schematic stretched view of the cut plane of the collector with a factor of 1 over 2 for the y- and x-axis. Magnetic field lines of the electron beam center (black), the electron beam thickness without sweeping (medium gray) and the electron beam thickness with sweeping (light gray).

upper end of the  $E \times B$  region and are each connected to a single rod. Each group of 5 rods is electrically and mechanically connected with metallic rings to distribute the electric potential in the complete structure. The  $E \times B$  structure is embedded in two ceramic rings at the top and bottom of the rods for mechanical support. The large insulator with flanges and both coils are modular gyrotron components at IHM/KIT and could be used for a concept prototype.

The magnetic field line of the electron beam center as well as the electron beam thickness in 2-D are shown in Fig. 2(b) for the SDC with and without an applied electric field sweeping potential. The magnetic field in the collector region above the electric field sweeping area was tuned to achieve a non-adiabatic transition of the electron beam for an increased beam thickness, although it should be noted that a non-adiabatic transition of the electron beam without sweeping is not sufficient for an acceptable power loading density at the collector wall. The intersection area of the electron beam with the collector wall is significantly increased with the electric field sweeping system, which is shown with the momentary and time-averaged power loading densities at the collector surface without considering space charge or secondary electron emission as shown in Fig. 3(a) and (b), respectively. The power loading distributions are only shown in a  $72^\circ$  segment due to the symmetry condition of  $n = 5$ . The maximum momentary power loading density is reduced from  $6 \text{ kW/cm}^2$  to  $4 \text{ kW/cm}^2$

in comparison to a traditional SDC with 200 mm inner radius for the KIT 2 MW 170 GHz coaxial-cavity gyrotron, which is a result of the shallower incident angle between the electron beam and the collector wall as well as the increased beam thickness due to the  $E \times B$  drift and the non-adiabatic transition. The maximum power loading density of the time-averaged wall loading is  $600 \text{ W/cm}^2$ , compared to the maximum acceptable averaged power loading density of conventional CW collectors with magnetic field sweeping is considered to  $500 \text{ W/cm}^2$ . Additional work must be done to verify that the increased heat flux is compatible with existing gyrotron collector cooling concepts.

An azimuthal density non-uniformity of the electron beam is a result of the azimuthal electron drift due to radial electric field components of the sweeping structure. An additional electric field is generated inside the electron beam with an azimuthal density non-uniformity with a similar shape to the electric field of the electric field sweeping electrodes [8]. Additional radial and azimuthal drift movements of the electrons will be observed when the space charge effect is included in the simulations. The momentary power loading density at the collector surface is slightly increased and shifted in phase in the positive azimuthal direction when the space charge effect is considered. The influence of the space charge is best visible in the angular power loading density shown in Fig. 3(c). The most challenging part of the electric field

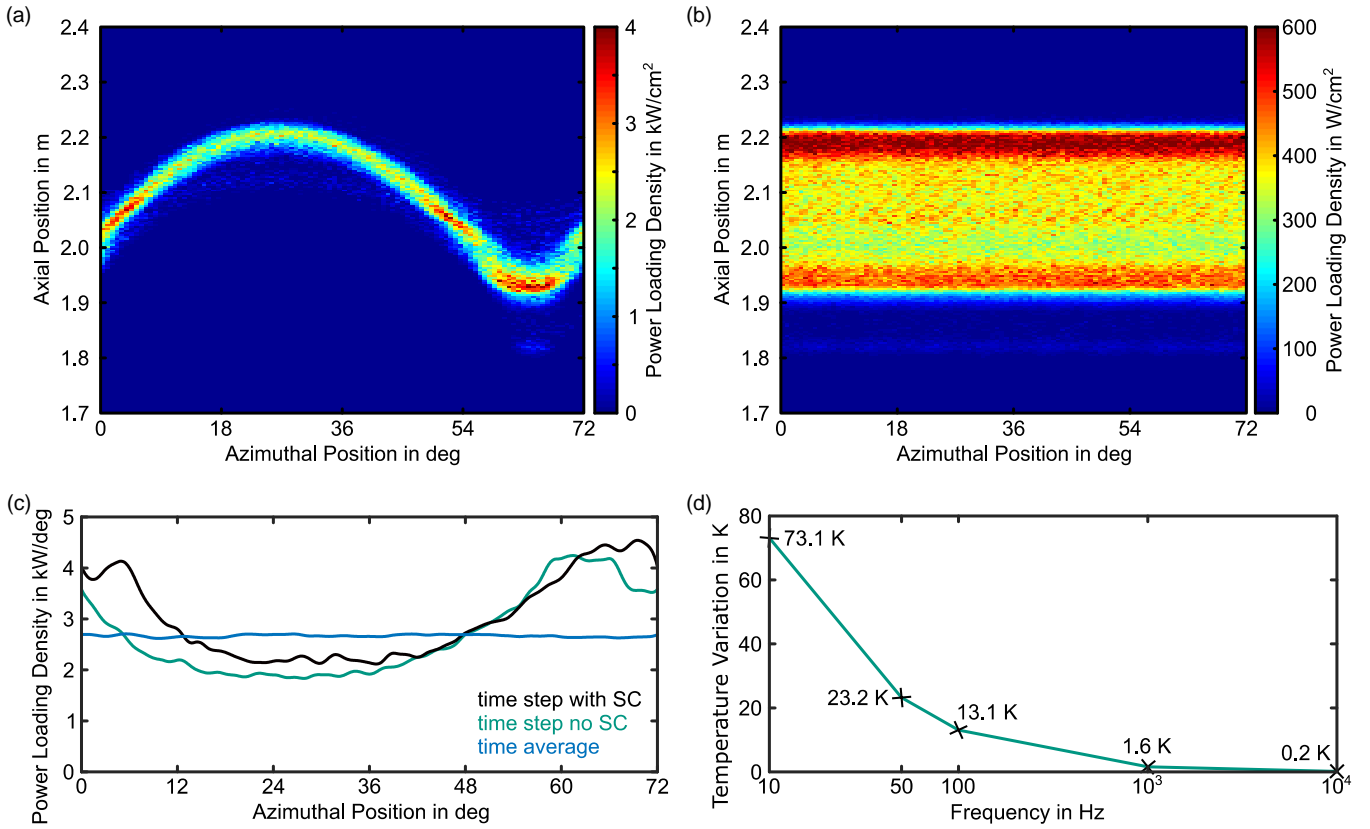


Fig. 3: Power loading at the collector surface. (a), Momentary power loading at the cylindrical collector at a 72 deg segment due to the symmetry of the periodic factor of  $n = 5$ . (b), Time average power loading density as a combination of 20 individual momentary time simulations at different phases of the sweeping system. (c), Angular power loading density for a momentary time step with Space Charge (SC), a momentary time step without SC and the time average power loading without SC. (d), Temperature variations at the inner collector wall for different sweeping frequencies.

sweeping system is the secondary electron emission (SEE). At the current state, a current is collected at the sweeping structure when SEE is considered. Future work must focus on the reduction of this current, as increased cooling of the sweeping structure, more than already necessary due to stray radiation inside the gyrotron, will increase the system complexity significantly.

## V. EFFECTS OF INCREASING SWEEPING FREQUENCY

The goal of the electric field sweeping system is an increased sweeping frequency for a reduced temperature variation at the inner collector surface. A reduced temperature variation correlates with an increased life expectancy of the collector due to reduced cyclic fatigue. Heat transfer simulations are performed for different sweeping frequencies. The power loading distribution of the spent electron beam, as shown in Fig. 3(a), is applied to the inner collector wall with a thickness of 10 – 20 mm. The outer collector wall is corrugated with 10 mm squared grooves to represent a HyperVapotron cooling structure as used in CW gyrotrons with heat transfer coefficients at the outside set to 23000 W/(m<sup>2</sup>·K) and around the groove to 8500 W/(m<sup>2</sup>·K) [9] with an external temperature of 20°C. The average temperature obtained at a sample point near the maximum power loading is between 370 – 380°C for all sweeping frequencies. However, the average temperature depends strongly on the heat transfer coefficient, which is not

well defined for HyperVapotron cooling. The temperature variation at the sample point is only slightly dependent on the correct heat transfer coefficient. The influence of the sweeping frequency on the temperature variations is much stronger due to the slow heat transfer through the collector wall material, which depends on the heat capacity and thermal conductivity of copper. Simulation results of the temperature variations at a sample point for different sweeping frequencies are shown in Fig. 3(d). The reduction in the temperature variation for a sweeping frequency over 10 kHz with a similar power loading distribution is very small. The temperature variation of the hottest point in a collector with LMFS and a 10 Hz triangular waveform in the sweeping coil usually ranges from 150 K and 200 K within one sweep cycle [10]. The temperature variation of a sample point in a collector with TMFS and 50 Hz sweeping should be slightly above the 23.2 K observed for the electric field sweeping due to an increased instantaneous power loading density.

It should be noted that the electric field in the cross-section of the  $E \times B$  region is very similar to a transverse electric field mode with the form  $TE_{n,1}$  in a circular waveguide. However, the outer boundary in the electric field sweeping system is not an electrical conductor thus the electric field lines are not orthogonal to the outer boundary. In theory, it should be possible to increase the electric field sweeping frequency until the cutoff frequency of the  $TE_{n,1}$  mode is reached. The lowest cutoff frequency in the collector region with 200 mm inner

radius for a  $TE_{n,1}$  is for  $n = 1$  at 439 MHz. The cutoff frequency for the  $TE_{5,1}$  as used in the conceptual design is at 1.53 GHz. However, the characteristic time  $\tau$  of the electrons in the electric field region must be taken into account for such high sweeping frequencies.

## VI. CONCLUSION

The mechanism of a novel electron beam sweeping system to reduce the collector fatigue in high-power vacuum tubes was presented and analyzed. A conceptual design for a 2 MW 170 GHz CW fusion gyrotron was presented as an example for this new type of electron beam sweeping system. A strong  $E \times B$  drift was achieved in the radial direction to alternate the axial position where the electron beam impinges the collector wall. To further amplify the sweeping effect, the static magnetic field in the collector region was optimized. The temperature variation at the inner collector wall is significantly reduced with increasing sweeping frequency. The lifetime of the collector can be significantly increased with this decreased cyclic fatigue.

## METHODS

**Analytical electron drift in 2D model.** The electron drift in the 2D cross-section, as shown in Fig. 1(b), is calculated analytically in MATLAB using sample electron beams. The characteristic time  $\tau$  of the electrons in the  $E \times B$  region is set to a value much larger than the limitation  $\tau \rightarrow 0$  set for Eq. (5) to achieve a significant drift distance. The calculation is performed in small iterative steps with a nearly constant electric field during the motion of the electrons. The electric field is then updated along with the new position of each electron. The kinetic energy of the sample electrons is considered to be relativistic to represent the spent electron beam of a gyrotron. However, only an axial velocity component is used for the initial electrons of the calculation.

**3D electron beam simulation.** The 3D simulations are performed in CST Studio Suite with the Particle Tracking Solver. The condition ( $T \gg \tau$ ) of a large period length of a sweeping cycle in relation to the characteristic time of an electron in the  $E \times B$  region must be fulfilled. The trajectory simulations are representative for a momentary time shot of the sweeping cycle.

**Momentary power loading on the collector surface.** The power loading on the collector surface is calculated in post-processing in MATLAB based on the trajectory simulation of CST. The collector surface is rasterized and the power of each cell is calculated as the sum of the power of all macro electrons incident on that cell.

**Time average power loading on the collector surface.** The time average power loading on the collector surface is calculated as the average of 20 individual momentary power loadings at different phases of the sweeping cycle.

## REFERENCES

- [1] G. Dammertz, S. Alberti, A. Arnold, E. Borie, V. Erckmann, G. Gantenbein, E. Giguet, R. Heidinger, J.P. Hogge, S. Illy, W. Kasperek, K. Koppenburg, M. Kuntze, H.P. Laqua, G. LeCloarec, Y. LeGoff, W. Leonhardt, C. Lievin, R. Magne, G. Michel, G. Müller, G. Neffe, B. Piosczyk, M. Schmid, K. Schwörer, M.K. Thumm, M.Q. Tran, "Development of a 140-GHz 1-MW continuous wave gyrotron for the W7-X stellarator," *IEEE Trans. on Plasma Sci.*, vol. 30, no. 3, pp. 808–818, June 2002, doi: 10.1109/TPS.2002.801509.
- [2] K. Felch, M. Blank, P. Borchard, P. Cahalan, S. Cauffman, T.S. Chu, H. Jory, "Recent ITER-Relevant Gyrotron Tests," *Journal of Physics: Conf. Series*, vol. 25, no. 3, pp. 13–23, 2005, doi: 10.1088/1742-6596/25/1/003.
- [3] M. Schmid, S. Illy, G. Dammertz, V. Erckmann, M. Thumm, "Transverse field collector sweep system for high power CW gyrotrons," *Fusion Engineering and Design*, vol. 82, no. 5–14, pp. 744–750, October 2007, doi: 10.1016/j.fusengdes.2007.06.008.
- [4] G. Dammertz, S. Illy, B. Piosczyk, M. Schmid, D. Bariou, "Collector sweeping systems for high power gyrotrons," *Joint 30th Int. Conf. on Infrared and Millimeter Waves and 13th Int. Conf. on Terahertz Electronics (IRMMW-THz)*, vol. 1, pp. 293–294, January 2006, doi: 10.1109/ICIMW.2005.1572524.
- [5] V. Erckmann, M. Schmid, H.P. Laqua, G. Dammertz, S. Illy, H. Braune, F. Hollmann, F. Noke, F. Purps, "Advanced gyrotron collector sweeping with smooth power distribution" 4th Int. Atomic Energy Agency technical meeting on ECRH physics and technology for ITER, pp. 1–5, January 2007.
- [6] I.Gr. Pagonakis, J.-P. Hogge, S. Alberti, K.A. Avramides, J.L. Vomvroidis, "A New Concept for the Collection of an Electron Beam Configured by an Externally Applied Axial Magnetic Field," *IEEE Trans. on Plasma Sci.*, vol. 36, no. 2, pp. 469–480, April 2008, doi: 10.1109/TPS.2008.917943.
- [7] T. Rzesnicki, B. Piosczyk, S. Kern, S. Illy, J. Jin, A. Samartsev, A. Schlaich, M. Thumm, "2.2-MW record power of the 170-GHz european pre-prototype coaxial-cavity gyrotron for ITER," *IEEE Trans. on Plasma Sci.*, vol. 38, no. 6, pp. 1141–1149, June 2010, doi: 10.1109/TPS.2010.2040842.
- [8] I.Gr. Pagonakis, J.L. Vomvroidis, "Evolution of an electron beam with azimuthal density nonuniformity in a cylindrical beam tunnel," *IEEE Trans. on Plasma Sci.*, vol. 32, no. 3, pp. 890–898, June 2004, doi: 10.1109/TPS.2004.827617.
- [9] S. Illy, S. Kern, I.Gr. Pagonakis, A. Vaccaro, "Collector Loading of the 2-MW, 170-GHz Gyrotron for ITER in Case of Beam Power Modulation," *IEEE Trans. on Plasma Sci.*, vol. 41, no. 10, pp. 2742–2747, October 2013, doi: 10.1109/TPS.2013.2262607.
- [10] B. Lyu, "Thermal investigation and lifetime estimation for the design improvement of a 2 MW fusion gyrotron collector," Master's thesis, Karlsruhe Institute of Technology, Karlsruhe, Germany, July 2020.